JOURNAL OF CATALYSIS **169,** 317–326 (1997)
ARTICLE NO. CA971702

Fluorinated Alumina Pillared α-Zirconium Phosphates as Supports for Metallic Nickel Catalysts

Josefa Mérida-Robles, Pascual Olivera-Pastor, Enrique Rodriguez-Castellón, and Antonio Jiménez-López[1]

Departamento de Química Inorgánica, Cristalografía y Mineralogía, Facultad de Ciencias, Universidad de Málaga, 29071 Málaga, Spain

Received December 23, 1996; revised March 3, 1997; accepted March 4, 1997

Two series of nickel catalysts supported on fluorinated alumina pillared α-zirconium phosphate materials have been prepared by the impregnation and ion-exchange methods, with metal loadings of 4, 10, 15, and 20 wt% for the former and 4 wt% for the latter. Temperature-programmed reduction profiles showed variable ranges of H_2 consumption, indicating that the reducibility of the Ni^{2+} species is dependent on nickel loading and support characteristics, such as alumina content and surface area. X-ray photoelectron spectroscopy analysis and reduction studies with H_2 indicated that a fraction of the loaded Ni^{2+} interacts with the support and cannot be reduced at $T < 873$ K. Samples were reduced at 773 and 873 K and their catalytic activity was probed in the reaction of hydrogenation of benzene. Despite the relatively low reduction and dispersion of metal found, the high-nickel-content catalysts displayed much higher activity than a reference Ni/Al_2O_3 catalyst. Conversion to cyclohexane was maximum, i.e., 100%, for samples reduced at 773 K containing 15 and 20 wt% Ni. Deactivation of these catalysts was imperceptible for at least 20 h on-stream.

INTRODUCTION

Much attention has been paid to the preparation and characterization of supported-nickel catalysts by their applications in many different industrial processes, such as hydrogenation (1), methanation (2), steam reforming (3), and hydrotreatment (4). Precedent studies have demonstrated consistently the importance of the support in determining essential characteristics of the active metal phase, such as reducibility of the metal ion, dispersion, active metallic surface, and sintering mechanisms. In other words, the activity of supported-nickel catalysts seems to be conditioned by the nature and properties of the support used. Oxides (Al_2O_3, SiO_2, TiO_2, etc.) and aluminosilicates (chiefly, zeolites and clay minerals) have been the supports commonly employed (5–8). Systematic studies have revealed that reduction and dispersion problems arise mainly from acid sites on the support surface and the extent and type of interaction between the support and the metal component. In particular, several authors have investigated the nature of the nickel–alumina interactions and have concluded that low reducibility and activity are caused by strong metal–support interactions. X-ray photoelectron spectroscopy (XPS) and X-ray diffraction (XRD) data have also revealed the presence of the compound $NiAl_2O_4$ on catalysts, which is formed on calcination at high temperatures (9–12). Likewise, the low reducibility observed in nickel–zeolite systems may be accounted for in terms of strong metal–support interactions as well (13, 14). Several strategies have been envisaged to overcome this inconvenience, for instance, calcining the alumina support at $T > 873$ K before contacting with the Ni^{2+} salt (15), and adding alkaline or transition metal ions (16–20).

The possibility of reducing the effects of nickel–alumina support interactions by using carriers with alumina diluted within another inorganic matrix has not yet been investigated, however. Alumina pillared layered compounds, in which aluminum oxide nanoparticles induce permanent porosity by propping apart the layers of a bidimensional host, could be, in principle, adequate candidates. In a recent work, we described the preparation and the surface properties of fluorinated alumina α-zirconium phosphate materials (21), finding that the presence of F^- improved significantly the thermal stability and porosity of alumina pillared α-zirconium phosphate. It is believed that this ion impedes uncontrolled formation of Al–O–P bonds during calcination, which otherwise would lead to stuffed structures. The aim of the present work was thus to study the effect of these pillared structures on reducibility, dispersion, and activity of supported-nickel catalysts. For this purpose, the catalysts were characterized using H_2 chemisorption, XPS analysis, and the hydrogenation of benzene as a test reaction.

EXPERIMENTAL

The supports chosen were two fluorinated alumina pillared α-zirconium phosphates, prepared as described elsewhere (21) and calcined at 673 K for 6 h. The calcined materials, with empirical formulas: $Zr[Al_{1.92}O_{0.64}\cdot(OH)_{2.04}F_{2.32}]H_{1.88}(PO_4)_2$ and $Zr[Al_{3.39}O_{1.12}(OH)_{1.60}F_{4.90}]\cdot H_{0.57}(PO_4)_2$ are hereafter referred to as AlZrP-0.5 and

[1] To whom correspondence should be addressed.

0021-9517/97 $25.00

AlZrP-1, respectively. Ni^{2+} was incorporated into the supports using both the incipient impregnation and ion-exchange methods. The former consisted of contacting the supports with ethyl alcohol solutions of $Ni(NO_3)_2$ corresponding to nickel loadings of 4, 10, 15, and 20 wt%. Ni^{2+}-exchanged samples were prepared using an aqueous solution of $Ni(NO_3)_2$ equivalent to 10 times the theoretical cation-exchange capacity of the original phosphate (6.6 meq/g), thereby providing a nickel loading of 4 wt%. For comparison, a 15 wt% Ni/Al_2O_3 reference sample was also prepared by the impregnation technique with a commercial alumina supplied by Repsol Petróleo S. A. All samples were then dried at 333 K and calcined at 723 K for 5 h.

Temperature-programmed reduction (TPR) of thermally treated impregnated samples was performed between 313 and 973 K, using a flow of Ar/H_2 (40 cm^3/min, 10% of H_2) and heating at 10 K/min. The water produced in the reduction reaction was eliminated by passing the gas flow through a cold finger (193 K). The consumption of reductor was controlled by an on-line gas chromatrograph provided with a TC detector. The degree of reduction of nickel (α) was determined by thermogravimetry using a CI Electronics microbalance, operating at an accuracy of 1 μg. In each run, 20 mg of sample, previously heated at 673 K under He flow (80 cm^3/min), was treated in a 10 vol% H_2–Ar flow (40 cm^3/min), heating at 10 K/min up to 773 or 873 K. The data were obtained measuring the weight loss due to the released water. Hydrogen chemisorption was used to determine the nickel dispersion, i.e., the surface Ni/total Ni ratio, using a conventional volumetric apparatus. The *in situ* reduction of catalyst was as follows: 450 mg of sample was heated at 10 K/min between 298 K and the reduction temperature chosen, and held 3 h at this temperature under a flow of 40 cm^3/min H_2/He (10% H_2). After reduction, samples were degassed at 10^{-6} Torr for 16 h at the same temperature and cooled to 298 K, to carry out chemisorption of H_2. The range of pressure studied in chemisorption was 5–100 Torr and the amounts of hydrogen chemisorbed were calculated by extrapolation of isotherms at $P = 0$ (22). Under the same experimental conditions, consumption of H_2 was nil on both supports.

Powder diffraction patterns (XRD) of samples were performed with a Siemens D501 diffractometer, provided with a graphite monochromator and using Cu $K\alpha$ radiation. XPS analyses were obtained with a Physical Electronics 5700 instrument with a Mg $K\alpha$ X-ray excitation source ($h\nu = 1253.6$ eV) and hemispherical electron analyzer. Accurate (± 0.1 eV) binding energies (BEs) were determined with respect to the position of the C 1*s* peak at 284.8 eV. The residual pressure in the analysis chamber was maintained below 10^{-9} Torr during data acquisition. Each spectral region of the photoelectrons of interest was scanned a number of times to obtain good signal-to-noise ratios. The catalysts were always handled under air-free conditions after the reduction step using the following procedure: the reduced samples, kept in a glass bulb provided with a stopcock, were transferred to a glove box, sealed in polyethylene bags under N_2, and deposited in the pretreament chamber under N_2 flow prior to XPS analysis. Transmission electron micrographs of the samples were obtained using a Philips CM 200 Supertwin-DX4 microscope. Samples were ultrasonically dispersed in ethanol; a drop of the suspension was put on a Cu grid (300 mesh) and covered with a Fornvar film.

The catalysts were tested in the benzene hydrogenation reaction at 443 K, using an automatic microcatalytic flow reactor under atmospheric pressure. The catalysts were supported on a glass frit located in the outlet arm of a U-shaped quartz reactor; the catalyst charge used was 60 mg without dilution. The catalysts were first reduced *in situ* at 873 or 773 K for 3 h in a flow of 40 cm^3/min H_2/He (10% H_2). The feed was a mixture of benzene and H_2 obtained by passing a flow of this gas through liquid benzene (chromatographic purity grade) held in a saturator–condenser kept at 303 K. A constant flow of 4.4 cm^3/min with a benzene concentration of 8.6% was maintained. The contact time was 59 g · h mol^{-1} and catalysts did not show diffusion restrictions. The reactor effluents were sampled via a microvolume sampling valve and injected into a gas chromatograph equipped with a flame ionization detector and a capillary column (TRB 1).

RESULTS

Characteristics of the Supports

To investigate the effects of the support properties on the activity of nickel catalysts, two supports with alumina contents of 21.4 and 29.3 wt% and surface areas of 130 and 184 $m^2\ g^{-1}$ were selected. These supports have basal spacings close to 17 Å (pillar height, $17 - 6.5 = 10.5$ Å), and a mixed porosity, essentially in the range of mesoporous but with a certain contribution of micropores ($V_{micro} \approx 0.1\ cm^3\ g^{-1}$), the average pore diameters being 58 and 37 Å for AlZrP-0.5 and AlZrP-1, respectively. The microporosity of these materials is considered to be induced by fluorinated alumina pillars within the phosphate interlayer region, whereas the mesoporosity is created principally by edge–edge and face–face interactions of the platelets. Total acidity, as measured by NH_3 temperature-programmed desorption (TPD), ranges between 1.7 and 1.5 mmol NH_3/g and pyridine adsorption data reveal that Lewis acid sites are the most abundant, having AlZrP-1 at twice the concentration of AlZrP-05. These materials are active for the dehydration of isopropyl alcohol, with activity values ranging between 11.7 and 23.7 μmol of propylene $g^{-1}\ s^{-1}$ (21). The main characteristics of the supports are summarized in Table 1. Since the supports display ion-exchange properties, Ni^{2+} was also loaded by ion exchange to establish the

TABLE 1

Characteristics of the Supports and Catalysts

Support	Ni (wt%)	S_{BET}[a] ($m^2\ g^{-1}$) 773 K[c]	S_{BET}[a] ($m^2\ g^{-1}$) 873 K[c]	V_{pore}[b] ($cm^3\ g^{-1}$) 773 K[c]	V_{pore}[b] ($cm^3\ g^{-1}$) 873 K[c]	Bulk Al/Ni molar ratio
AlZrP-1	0	184.0		0.17		
	10	—	85.5	—	0.14	3.04
	15	96.8	90.6	0.14	0.17	1.90
	20	89.3	74.4	0.12	0.11	1.34
AlZrP-05	0	130.0		0.19		
	10	—	68.9	—	0.11	2.22
	15	64.3	53.8	0.10	0.10	1.40
	20	72.2	67.2	0.11	0.12	0.98
Al_2O_3	0	302.0		0.33		
	15	—		—		6.52

[a] BET method.
[b] Accumulated pore volume.
[c] Temperature of reduction.

influence of the preparation method on the properties of the supported-nickel catalysts.

Calcined Precursor Samples

The presence of NiO on the surface of the supports after calcination was confirmed by XRD and XPS. The characteristic diffraction lines of NiO appear at 2.41 and 2.09 Å, and their intensities increase with nickel loading, as expected. For both series of materials, the Ni $2p_{3/2}$ spectra (Fig. 1) show a main peak, characteristic of Ni^{2+}, which shifts to lower BE values from 856.1 to 855.1 eV and becomes wider at higher nickel loading. This peak could be deconvoluted into two components, one centered at 854.1 eV and the other at 856.1 eV. Taking into account that the BE for unsupported NiO is 853.5 eV, the peak at 854.1 eV may be assigned to Ni^{2+} in octahedral sites of the supported NiO structure, and the peak at 856.1 eV may then be associated with Ni^{2+} in tetrahedral positions of a spinel-like structure of Ni–Al oxide, created as a result of the solid-state diffusion of Ni^{2+} into the alumina lattice (9). The peak located at 862 eV, which essentially remains in the same position, corresponds to the shakeup satellite structure of Ni^{2+}. The distribution of Ni^{2+} on the support surface was determined by plotting the Ni/Zr surface ratio, obtained by XPS, vs Ni content (Fig. 2). For both series of materials, the values lie close to a straight line, indicating that the oxidic phase is homogeneously distributed on the support.

The TPR profiles of impregnated samples are variable according to the nickel loading (Fig. 3). Thus, samples with the lowest content (4 wt%) show only a broad peak with a maximum at 863 K, but at higher Ni^{2+} loading, a new peak with increasing relative intensity appears at lower temperature (near 700 K), becoming the most intense at the highest loading. The sample with 20 wt% Ni^{2+} shows only small shoulders beyond 750 K. TPR profiles are quite similar for

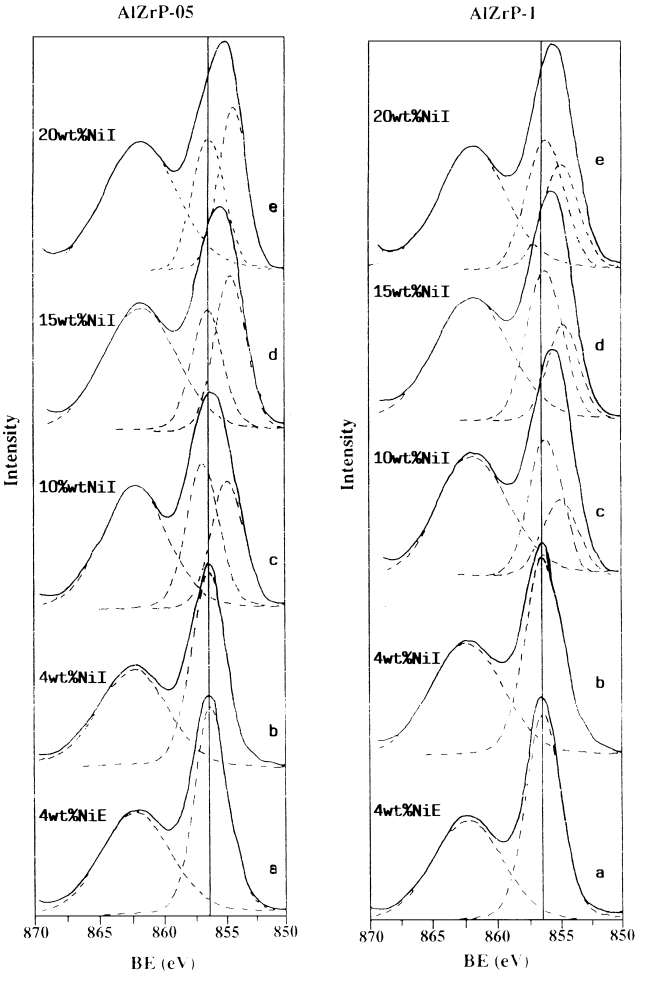

FIG. 1. Ni $2p_{3/2}$ XPS spectra of calcined precursors prepared by ion exchange (E) or impregnation (I).

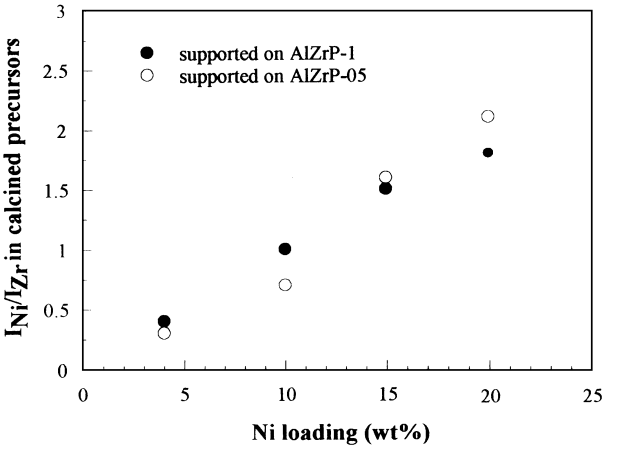

FIG. 2. Variation of the Ni : Zr ratio as a function of the nickel loading in calcined precursors.

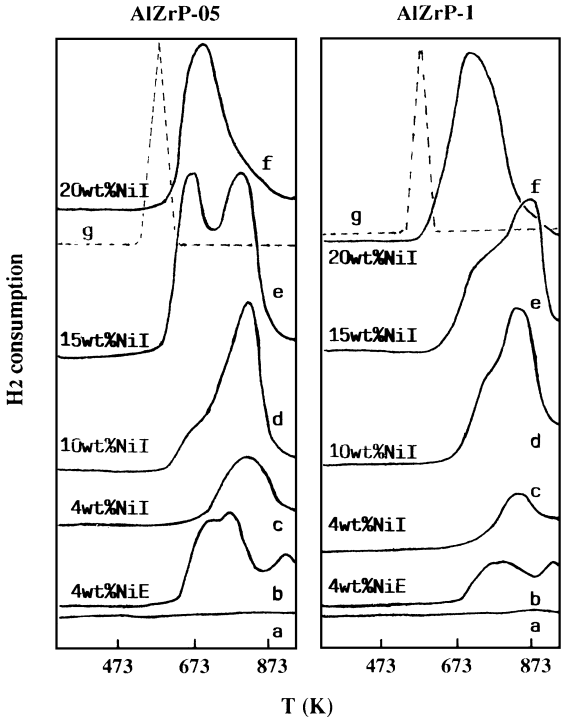

FIG. 3. TPR profiles of the supports (a), unsupported NiO (g), and supported nickel catalysts (b–f). E, exchanged; I, impregnated.

both supports, although the reduction temperatures and the relative intensities of peaks are slightly different. Ni^{2+}-exchanged samples exhibit three defined ranges of hydrogen consumption, with maxima at 763, 808, and 943 K. The existence of several defined ranges of H_2 consumption in TPR profiles points to the presence of more than one Ni^{2+} species in calcined precursors.

Supported-Nickel Catalysts

Given that the Ni^{2+}–support interaction affects the reducibility of precursors, treatment with H_2 was carried out at two different temperatures. Evidence of the formation of nickel metallic particles on the support surface, after treatment with H_2, was again provided by XRD and XPS analysis. The XRD patterns show the characteristic diffraction lines of Ni^0 at 2.03 and 1.76 Å; however, such particles were not observed in 4 wt% Ni samples, in which Ni^{2+} ions should be extremely dispersed and strongly interacting with the substrate before reduction. No significant changes in the surface properties of the supports were observed at low nickel loading; however, at high loading, the presence of nickel metallic particles modifies the sintering of the pillared phosphate support giving rise to a decrease in the BET surface area and pore volume (Table 1). In addition, the metal particles may also partially block the access of N_2 molecules to the support internal pores. Note that the bulk Al/Ni molar ratio in the alumina pillared phosphate-supported nickel catalysts (Table 1) is much lower (0.98–3.04) than that in the reference alumina-supported catalyst (6.52). Thermogravimetric measurements of degree of reduction (α) in the catalysts are compiled in Table 2. For both series of catalysts, α increases with Ni loading and reduction temperature, although complete reduction was not achieved for any sample.

Table 3 compares BE values and P/Zr and Al/Ni surface atomic ratios in Ni^{2+}-impregnated samples before and after reduction with hydrogen. Practically constant BE values of Zr 3*d* and P 2*p* core electrons, together with the fact that the P/Zr atomic ratio is close to the theoretical value, P/Zr = 2, suggest that the host framework was not altered during the impregnation–calcination–reduction process. Instead of two signals corresponding to Ni^{2+} species

TABLE 2

Properties of Supported Nickel Catalysts

Support	Ni (wt%)	$T_{reduction}$ (K)	α	D (%)	Metal area[a] $(m^2\ g^{-1})_{Ni^0}$	d (nm)		Activity[b] $(\mu mol/s\ g)_{Ni^0}$
						H_2 adsorption	XRD	
AlZrP-1	20	873	0.91	0.43	2.87	136.4	—	15.7
	15	873	0.73	1.09	7.29	42.9	53.9	18.0
	10	873	0.50	1.64	10.93	19.7	19.9	32.0
	20	773	0.51	1.06	7.05	31.1	34.8	40.9
	15	773	0.35	3.62	24.10	6.3	—	78.9
AlZrP-05	20	873	0.89	0.50	3.22	118.6	84.4	10.7
	15	873	0.85	0.53	3.42	107.4	31.0	9.2
	10	873	0.82	0.59	3.84	92.4	31.2	13.1
	20	773	0.65	0.92	6.00	46.7	40.0	19.0
	15	773	0.45	2.27	14.74	13.16	—	26.5
Al_2O_3	15	873	0.32	3.6	23.4	5.9	—	20.3

[a] From H_2 adsorption isotherms at 298 K.
[b] Activity (μmol s^{-1} per accessible Ni^0/g).

TABLE 3

Binding Energy (BE), Surface Atomic Ratio and Reduction Degree as Determined by XPS Analysis

Support	Ni (wt%)	BE (eV)						Atomic ratio on surface		% Ni^0 (XPS)
		Zr $3d_{5/2}$	O 1*s*	P $2p_{3/2}$	Al 2*p*	Ni^{2+} $2p_{3/2}$	Ni^0 $2p_{3/2}$	P/Zr	Al/Ni	
Unreduced catalysts										
AlZrP-1	0	183.4	531.5	134.1	75.8			2.0		
	20I	183.0	531.5	134.1	74.8	856.0–854.8		2.0	3.8	
	15I	182.7	531.4	134.0	74.6	856.1–854.6		1.9	4.2	
	10I	182.9	531.5	134.1	74.6	856.2–854.6		2.0	7.0	
	4I	183.0	531.6	134.1	74.8	856.4		1.9	17.0	
	4E	183.0	531.4	133.8	74.6	856.2		1.9	9.1	
AlZrP-05	0	184.5	532.1	134.5	75.2			2.2		
	20I	183.0	531.9	134.0	74.0	856.0–854.1		2.3	1.8	
	15I	183.0	531.5	133.9	74.9	856.4–854.5		2.4	2.1	
	10I	183.1	531.6	134.0	74.9	856.6–854.5		2.2	5.0	
	4I	183.0	531.6	134.2	74.7	856.5		2.3	12.0	
	4E	182.6	531.1	134.0	74.5	856.2		2.1	5.8	
Reduced catalysts at 873 K										
AlZrP-1	20I	182.7	531.2	134.1	74.7	856.0	852.7	2.1	7.9	19.7
	15I	183.0	531.6	134.2	74.8	855.8	852.3	2.1	7.5	20.7
	10I	182.9	531.7	134.5	75.0	855.8	853.5	2.1	13.4	10.1
AlZrP-05	20I	183.1	531.9	134.6	75.1	855.8	852.7	2.3	4.8	26.2
	15I	183.0	531.5	133.9	74.9	856.0	853.2	2.3	13.6	22.8
	10I	183.2	531.9	134.5	75.1	855.7	852.4	2.4	11.7	27.9
Reduced catalysts at 773 K										
AlZrP-1	20I	182.9	531.2	134.0	74.9	855.8	852.5	1.9	6.6	19.3
	15I	183.6	532.2	134.9	75.5	855.9	853.0	2.0	7.7	17.7
AlZrP-05	20I	183.2	532.0	134.5	75.0	855.3	852.3	2.2	3.6	22.5
	15I	183.0	531.6	134.4	74.9	856.2	853.6	1.9	3.4	20.0

appearing at Ni loading > 10%, the XPS spectra of reduced samples (Fig. 4) show only a single signal for Ni^{2+} in the range 855.3–856.2 eV, which closely corresponds to the higher-energy peak in the spectra of unreduced samples. This means that the fraction of Ni^{2+} that strongly interacts with the support cannot be reduced below 873 K. The peak position of unreduced Ni^{2+} species is ca. 2 eV higher than that corresponding to unsupported NiO and close to that corresponding to tetrahedral Ni^{2+}. In addition, a new peak appears in the XPS spectra of reduced samples at 852.3–853.6 eV, which is indicative of the presence of Ni^0. The presence of Ni^{2+} species on the support surface lowers the BE of Al 2*p* core electrons, probably as a consequence of the Ni^{2+}–alumina pillar interaction. The BE of Al 2*p* core electrons is higher in reduced than in unreduced samples, but still lower than that characteristic of the support, which may be due to the presence of a fraction of unreduced nickel after treatment with H_2. From XPS data, percentages of Ni^{2+} reduction on the support surface were calculated (Table 3) as the ratio of the integrated peak area of Ni metal to the entire Ni peak area (including the satellite peak). The percentage of reduced Ni phase increased with nickel content, but no more than 26.2% reduction was achieved by this method. A decrease in the surface Ni/Zr ratio was observed after reduction with H_2 (Fig. 5) as a consequence of the agglomeration of nickel atoms forming metallic particles. Therefore, as nickel atoms in the bulk of a particle will not contribute to the Ni^0 signal, low degrees of reduction should be expected by XPS (23). Nevertheless, the plot in Fig. 5 suggests that nickel particles in the support AlZrP-05, with lower surface area and alumina content, are larger than those in the support AlZrP-1, as larger deviations from the initial ratio were observed for the former.

Percentage of metal exposed, metallic surface area, and particle size were determined using hydrogen chemisorption data at 298 K (Table 2). Under the experimental conditions used, no chemisorption of H_2 was detected on the supports. Typical hydrogen chemisorption isotherms on reduced samples are shown in Fig. 6. As can be seen hydrogen chemisorption was higher in the catalysts reduced at lower temperature; in addition, a decrease in hydrogen uptake was observed on increasing nickel loading from 10 to 20 wt%. Dispersion degree (*D*) was calculated taking into account the extent of reduction and assuming a stoichiometry H/Ni = 1 (24). The *D* values for AlZrP-1-supported catalysts (0.43–3.62%) were usually higher than

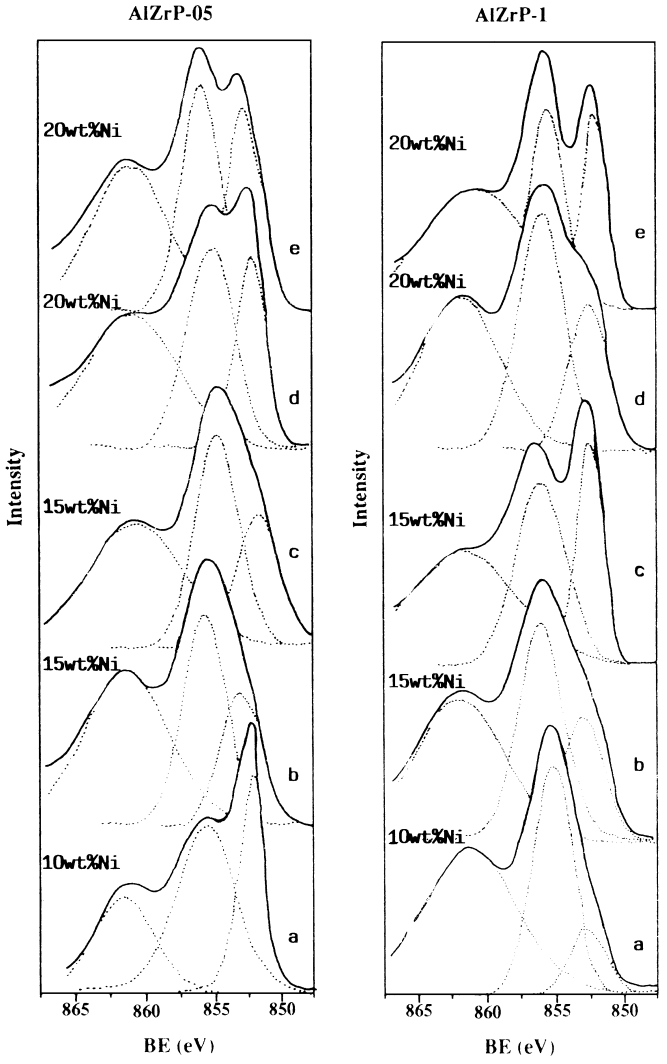

FIG. 4. Ni $2p_{3/2}$ XPS spectra of reduced catalysts at 873 K (a, c, e) and 773 K (b, d).

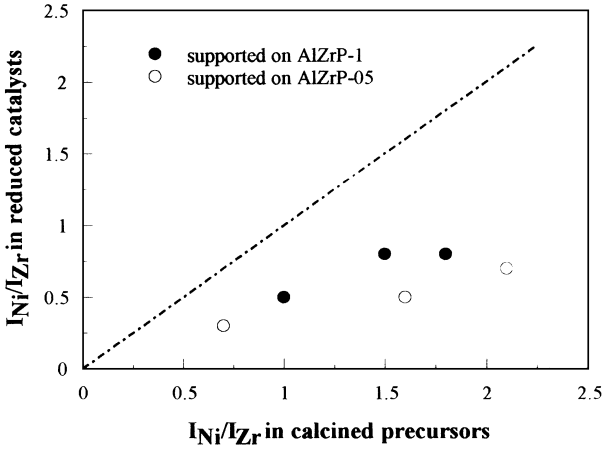

FIG. 5. Relationship between the Ni : Zr surface ratios for reduced and calcined catalysts.

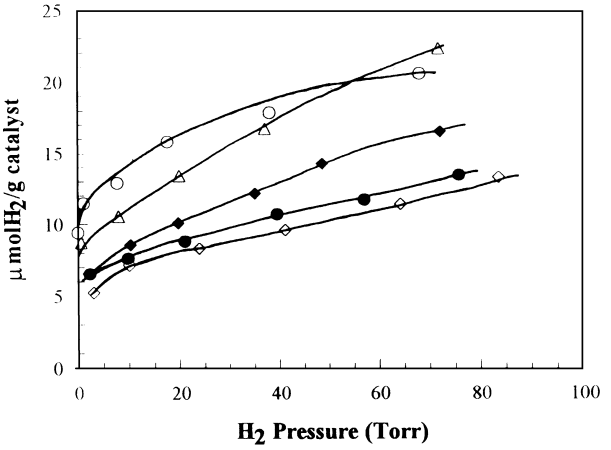

FIG. 6. H_2 chemisorption isotherms on reduced catalysts at 298 K. Support AlZrP-1: 20 wt% Ni ($T_R = 773$ K) (△), 20 wt% Ni ($T_R = 873$ K) (●), 10 wt% Ni ($T_R = 873$ K) (◆). Support AlZrP-05: 15 wt% Ni ($T_R = 773$ K) (○), 15 wt% Ni ($T_R = 873$ K) (◇).

those for AlZrP-05-supported catalysts (0.50–2.27%), in part because the available surface area for Ni^{2+} ions was higher for the former support. For both series of catalysts, dispersion degree was higher at 773 K than at 873 K, whereas the reduction percentage was lower at lower temperature, which means that sintering of nickel particles is more effective at higher temperatures of reduction. The dispersion degree values found here were similar to those of alumina supports (11), but quite lower than those for other supports (5, 19, 23). Metallic surface area, S_m, was determined from dispersion degree using a value of 6.33 Å^2 as the cross-sectional area of the nickel atom. Average nickel particle size (d) was obtained from the equation $d = 431\alpha/S_m$, generally applied to hemispherical particles of metal, pressumed to be formed in systems where interactions between metal and the support occur (25). Calculated particle sizes (Table 2) were greater at higher temperatures of reduction and for the catalysts with the support of lower BET surface area (AlZrP-05). At $T_R = 873$ K, the particle diameters were close to 100 nm for catalysts supported on AlZrP-05, whereas for catalysts supported on AlZrP-1, values ranging between 20 and 136 nm were found. Reduction at 773 K gave rise to smaller nickel particles for both series of catalysts, ranging between 6 and 47 nm. These data were in good agreement with those observed by TEM (Fig. 7). For comparison, average particle diameter was also calculated from XRD measurements. This method provided values close to those found from H_2 adsorption for the AlZrP-1 catalysts series, but generally lower than those for the AlZrP-0.5 catalysts series (Table 2).

The hydrogenation of benzene has been chosen to probe the activity of these supported-nickel catalysts. This reaction has been widely used for the characterization of supported-metal catalysts, including the determination of percentage of metal exposed (26). Conversion data is

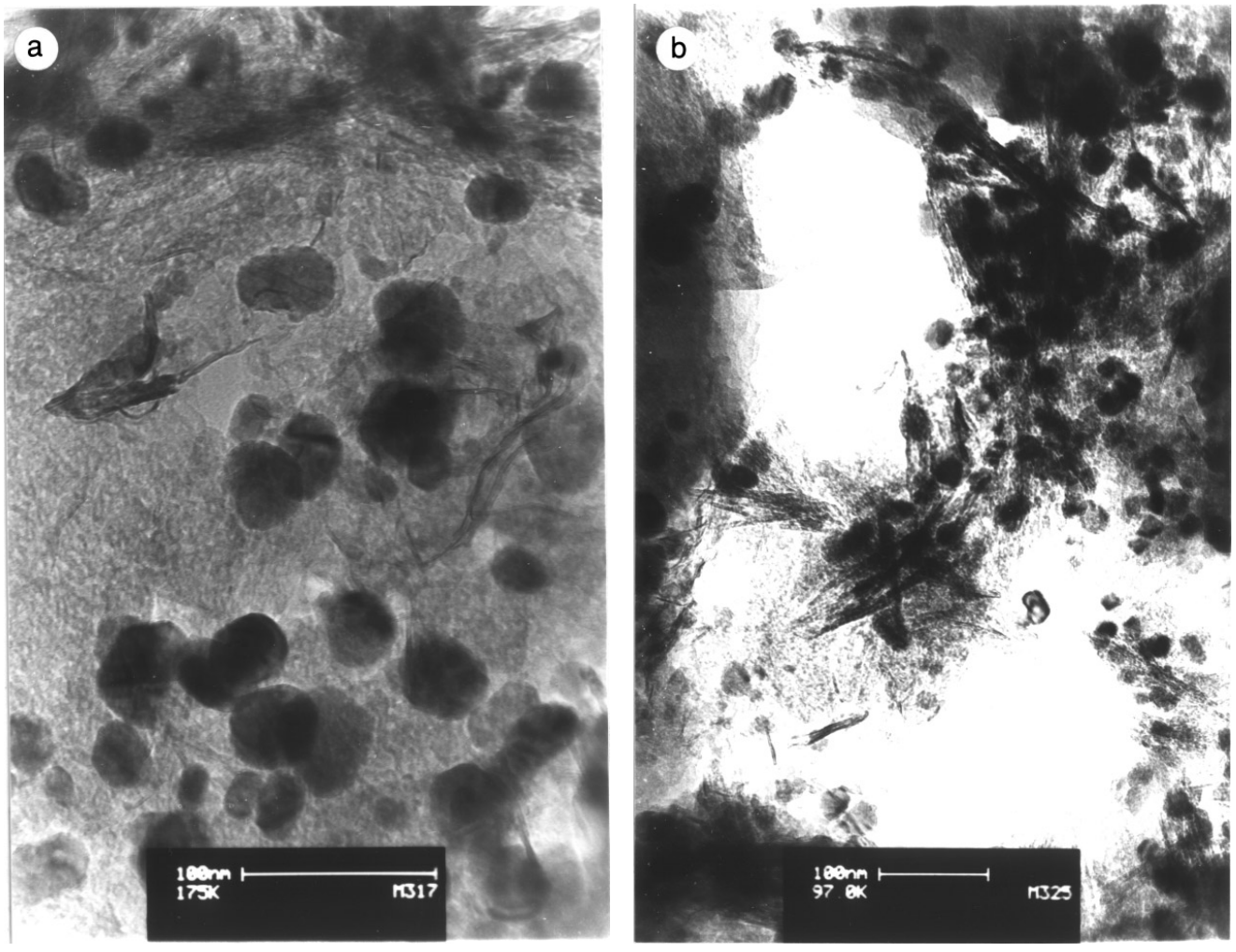

FIG. 7. Transmission electron micrographs of AlZrP-1-supported nickel catalysts reduced at 873 K: 10 wt% Ni (a) and 15 wt% Ni (b). Bar = 100 nm.

plotted versus time on-stream in Fig. 8. Materials with nickel loading lower than 10% were poorly active for this reaction. Cyclohexane was the only reaction product, and therefore, the selectivity was 100%. Catalysts obtained at 873 K reached a steady state later (15 h on-stream) than those prepared at 773 K (before 2 h). Percentage conversion ranged from 50 to 100% for AlZrP-1 and from 40 to 100% for AlZrP-05. In both series of catalysts, conversion increases with nickel loading and is maximum, i.e., 100%, for samples reduced at 773 K with Ni loadings of 15 and 20 wt%. These conversion values were much higher than those observed for nickel catalysts supported on zeolites (8) and silica pillared phosphates (27). Activity data, in μmol/s · g(Ni^0), are listed in Table 2. As expected, these values are clearly dependent on the degree of dispersion; thus, higher D values result in higher activities (support AlZrP-1), whereas nearly constant D values lead only to slight variations in activity (support AlZrP-05, $T_R = 873$ K). Significantly, the reference 15 wt% Ni/Al_2O_3 catalyst showing reduction degree, dispersion, metal area, and particle size very similar to those of the corresponding nickel catalysts supported on AlZrP-1 (15 wt% Ni, $T_R = 773$ K) presented, however, much lower activity values (Table 2).

DISCUSSION

Although α-zirconium phosphate displays a very high cation-exchange capacity (6.6 meq g^{-1}), it is considerably reduced by the presence of fluorinated alumina pillars in the interlayer region. Thus, only small amounts of nickel could be loaded onto the supports by the ion-exchange method, 4 wt% as maximum. The exchange sites come from hydroxyl groups attached to the phosphate layer and/or belonging to the alumina pillar, but, even though the pillar densities were different, both supports showed apparently the same exchange capacity. Therefore, a high dispersion of Ni^{2+} ions on the support surface should be expected in low-Ni^{2+}-loaded samples. In fact, no formation

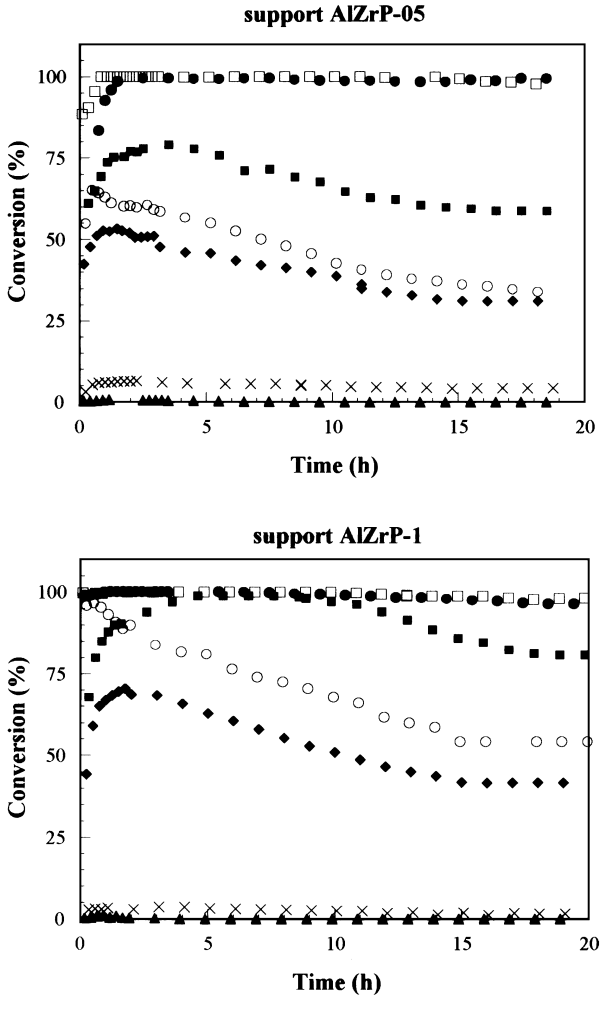

FIG. 8. Variation of the percentage conversion in benzene hydrogenation as a function of time on-stream $T_R = 773$ K: 20 wt% Ni I (□), 15 wt% Ni I (●); $T_R = 873$ K: 20 wt% Ni I (■), 15 wt% Ni I (○), 10 wt% Ni I (◆), 4 wt% Ni I (×), 4 wt% Ni E (▲).

of NiO could be detected by XRD on calcining 4 wt% Ni samples.

According to TPR profiles, the reduction temperature of Ni^{2+} on the surface of fluorinated alumina pillared materials is, in all cases, higher than that corresponding to unsupported NiO (616 K). Consequently, interaction between Ni^{2+} species and the support occurs. XPS data and TPR profiles suggest that Ni^{2+} is present in, at least, two different environments in calcined precursors with nickel loading > 4 wt%, i.e., forming part of the NiO network and as dispersed ions in exchange positions. Thus, XPS measurements gave a higher Al/Ni ratio on the surface of calcined precursors, because a fraction of dispersed Ni^{2+} ions may be located on internal alumina pillar walls. H_2 consumption at very high temperature is indicative of the existence of highly dispersed Ni^{2+} strongly interacting with the support. The formation of NiO and Ni–Al oxide spinel has been reported for several nickel catalysts supported on alumina (7–10). These species fixed to the support differ in reducibility and their relative concentrations depend on the nickel content, the nature of the support, and the calcination temperature (9–12). According to the literature (28), Ni^{2+} in a spinel-like structure is more difficult to reduce, hence the high-temperature TPR peak(s) might be tentatively associated with this species. The lower-temperature TPR peak(s) may be associated with NiO, which interacts to a lesser extent with the support. On increasing nickel loading, the amount of deposited NiO increases and the interaction of the outer NiO overlayer with the support decreases. Thus the corresponding TPR peak shifts to lower temperature at high nickel percentages (15 and 20 wt%). Consequently, the reduction of supported NiO become easier at higher nickel loadings. The low reducibility of nickel as related to its high dispersion has been also observed in other systems like Ni^{2+}–Y zeolites, where reduction and agglomeration of Ni^{2+} are very difficult (13, 14). Also, the surface characteristics of the support affect the reducibility of nickel oxide; the reduction temperature is thus lower when the oxide is supported on AlZrP-0.5, which has a lower alumina content and surface area and, therefore, the interaction with the support and the degree of dispersion of Ni^{2+} species should be lower. This is corroborated by the fact that the XPS signal corresponding to reducible NiO is more intense for the support AlZrP-0.5 (Fig. 1). In general, the reduction temperature of Ni^{2+} is higher for the alumina pillared supports than for analogous silica pillared materials (27) and is within the range of systems where interaction between nickel species and the support occurs (15).

The degree of reduction (α) varied between 0.5 and 0.9 at $T_R = 873$ K and between 0.35 and 0.65 at $T_R = 773$ K (Table 2). The relative low α values obtained may be justified by the presence of an important fraction of Ni^{2+} that interacts with the alumina pillared surface and is very difficult to reduce and nucleate (15). Thus, α is generally lower for the support AlZrP-1, where the Al/Ni ratio is higher, and hence, the Ni^{2+}–support interaction takes place to a greater extent, as corroborated by XPS. With respect to particle size, good agreement between H_2 chemisorption and XRD measurements was observed for nickel catalysts supported on AlZrP-1, whereas for the AlZrP-0.5 series, H_2 adsorption provided higher values for crystallite size, especially for samples containing 10 and 15 wt% Ni. An overestimation of particle size from H_2 adsorption has been interpreted in the literature (29) as being due to a strong metal–support interaction (SMSI). Although the SMSI state should not be ruled out, XPS measurements suggest the presence of relatively larger amounts of reducible NiO (Fig. 1) and larger nickel particles (Fig. 5) on the support AlZrP-0.5. It is also possible that, for AlZrP-0.5-supported nickel catalysts, XRD data could represent average crystalline domain sizes rather than crystallite sizes.

In this study, benzene hydrogenation was used for the characterization of reduced metal centers. Only catalysts containing 10–20 wt% Ni displayed significant activity for this reaction. The low activity of materials with lower nickel loading was expected from previous XPS and XRD studies, since nickel particles could hardly be detected. The direct correlation observed between activity and metal dispersion indicates that the reaction is structure insensitive, although no direct evidence could be obtained because of the variability of the conversion values. Given that the activity for the AlZrP-1 catalyst series was higher than for the AlZrP-0.5 series, the former would be expected to have a smaller particle size, as suggested by H_2 adsorption measurements. The higher conversion observed at 773 K may be also related to the fact that, at this temperature, the degree of dispersion is higher and the particle size is smaller.

Compared with the reference Ni/Al_2O_3 catalyst, the nickel catalysts supported on fluorinated alumina pillared phosphate materials displayed noticeable enhanced activity for the hydrogenation of benzene. This can be attributed to the fact that the nickel–support interaction is much stronger for the alumina support, in which the Al/Ni ratio is much higher (6.52 against 1.90). Indeed, not only the dilution effect of alumina on the support but also the strong alumina pillar–phosphate interaction might be responsible for the lower interaction between nickel particles and pillared phosphates. It has been demonstrated that a change in the electron density of the metal can significantly modify chemisorption and catalytic properties (20). Furthermore, nickel catalysts supported on fluorinated alumina pillared α-zirconium phosphates could be easily regenerated by oxidation in air and further reduction under the same conditions or simply by treatment with a H_2/He flow at 773 K (Fig. 9).

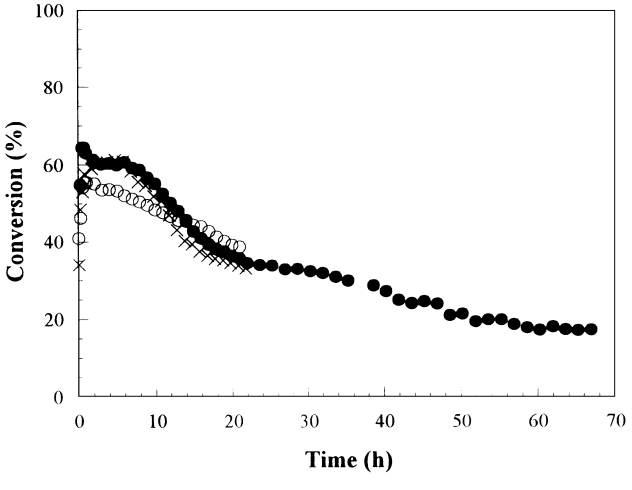

FIG. 9. Conversion (%) in benzene hydrogenation versus time on-stream for the AlZrP-05-supported 15 wt% Ni catalyst reduced at 873 K (●) and after calcination in air and regeneration with a H_2/He flow at 873 K (○) or regeneration with H_2/He flow at 873 K (×).

CONCLUSIONS

Fluorinated alumina pillared α-zirconium phosphate materials have been shown to be appropriate supports for preparing nickel catalysts. Dispersion of alumina, as pillaring oxide in the interlayer region of α-zirconium phosphate, seems to decrease the interaction with nickel particles, thereby giving rise to highly active catalysts for the hydrogenation of benzene. In particular, samples reduced at 773 K with nickel loadings of 15 and 20 wt% displayed the maximum conversion (100%), which was maintained for a relatively long time on-stream (at least 20 h). In addition, regeneration of the catalyst could be achieved without apparent loss of activity.

ACKNOWLEDGMENTS

This research was supported by CYCIT (Spain) Project MAT94-0678 and by E.U. Programme BRITE-EURAM Contract BRE2-CT93-0450.

REFERENCES

1. Coenen, J. W. E., *Ind. Eng. Chem. Fundam.* **25**, 43 (1986).
2. Ross, J. R. H., *in* "Specialist Periodical Reports, Catalysis," Vol. 7, p. 1. Roy. Soc. of Chem., London, 1985.
3. Bridger, G. W., *in* "Specialist Periodical Reports, Catalysis," Vol. 3, p. 39. Roy. Soc. of Chem., London, 1983.
4. Ledoux, M. J., *in* "Specialist Periodical Reports, Catalysis," Vol. 7, p. 125. Roy. Soc. of Chem., London, 1985.
5. Narayanan, S., and Skeekanth, G., *J. Chem. Soc. Faraday Trans. 1* **85**(II), 3785 (1989).
6. Hoang-Van, C., Kachaga, Y., Teichner, S. J., Arnaud, Y., and Dalmon, J. A., *Appl. Catal.* **46**, 281 (1989).
7. Coenen, J. W. E., *Appl. Catal.* **75**, 193 (1991).
8. Daza, L., Pawelec, B., Anderson, J. A., and Fierro, J. L. G., *Appl. Catal. A* **87**, 145 (1992).
9. Wu, M., and Hercules, D. M., *J. Phys. Chem.* **83**(15), 2003 (1979).
10. Scheffer, B., Molhock, P., and Moulijn, J. A., *Appl. Catal.* **46**, 11 (1989).
11. Gil, A., Díaz, A., Gandía, L. M., and Montes, M., *Appl. Catal. A* **109**, 167 (1994).
12. Gandía, L. M., and Montes, M., *J. Mol. Catal.* **94**, 347 (1994).
13. Minchev, Ch., Knarizer, V., Kosova, L., Pechev, V., Grunsser, W., and Schmidt, F., *in* "Proceedings, 5th Conference on Zeolites" (L. V. C. Rees, Ed.), p. 335. Heyden, London, 1980.
14. Suzuki, M., Tsutsumi, K., and Takahashi, H., *Zeolites* **2**, 87 (1982).
15. Lindfors, L. P., and Smeds, S., *Catal. Lett.* **28**, 291 (1994).
16. Narayanan, S., and Uma, K., *J. Chem Soc. Faraday Trans. 1* **81**, 2733 (1985).
17. Houalla, M., Lemaitre, J., and Delmon, B., *J. Chem. Soc. Faraday Trans. 1* **78**, 1389 (1982).
18. Narayanan, S., and Uma, K., *J. Chem Soc. Faraday Trans. 1* **83**, 733 (1987).
19. Narayanan, S., and Uma, K., *J. Chem Soc. Faraday Trans. 1* **84**(2), 521 (1988).
20. Sauvion, G. N., Tempere, J. F., Guilleux, M. F., Djega-Mariadassou, G., and Delafosse, D., *J. Chem. Soc. Faraday Trans. 1* **81**, 1357 (1985).
21. Mérida-Robles, J., Olivera-Pastor, P., Jiménez-López, A., and Rodriguez-Castellón, E., *J. Phys. Chem.* **100**(35), 14726 (1996).

22. Wilson, G. R., and Hall, W. K., *J. Catal.* **17**, 190 (1970).
23. Anderson, J. A., Daza, L., Fierro, J. L. G., and Rodrigo, M. T., *J. Chem. Soc. Faraday Trans.* **89**(19), 3651 (1993).
24. Scholten, J. J. F., Pijpers, A. P., and Hustings, A. M. L., *Catal. Rev. Sci. Eng.* **27**, 151 (1985).
25. Coenen, J. W. E., and Linsen, B. G., *in* "Physical and Chemical Aspects of Adsorbents and Catalysts" (B. G. Linsen, Ed.), p. 495. Academic Press, London, 1970.
26. Fajardie, F., Tempére, J. F., Mariadassou, G. D., and Blanchard, G., *J. Catal.* **163**, 77 (1996).
27. Santamaría-González, J., Martínez-Lara, M., and Jiménez-López, A., *J. Chem. Soc. Faraday Trans.* **93**(3), 493 (1997).
28. Rynkowski, J. M., Paryjczal, T., and Lenik, M., *Appl. Catal.* **106**, 73 (1993).
29. Hoang-Van, C., Kachaya, Y., Teichner, S. J., Arnaud, Y., and Dalmon, J. A., *Appl. Catal.* **46**, 281 (1989).